ELSEVIER

Journal of the Mechanics and Physics of Solids
52 (2004) 567–589

JOURNAL OF THE
MECHANICS AND
PHYSICS OF SOLIDS

www.elsevier.com/locate/jmps

Eshelby problem of polygonal inclusions in anisotropic piezoelectric full- and half-planes

E. Pan*

Department of Civil Engineering, The University of Akron, Akron, OH 44325-3905, USA

Received 9 January 2003; received in revised form 4 August 2003; accepted 4 August 2003

Abstract

This paper presents an exact closed-form solution for the Eshelby problem of polygonal inclusion in anisotropic piezoelectric full- and half-planes. Based on the equivalent body-force concept of eigenstrain, the induced elastic and piezoelectric fields are first expressed in terms of line integral on the boundary of the inclusion with the integrand being the Green's function. Using the recently derived exact closed-form line-source Green's function, the line integral is then carried out analytically, with the final expression involving only elementary functions. The exact closed-form solution is applied to a square-shaped quantum wire within semiconductor GaAs full- and half-planes, with results clearly showing the importance of material orientation and piezoelectric coupling. While the elastic and piezoelectric fields within the square-shaped quantum wire could serve as benchmarks to other numerical methods, the exact closed-form solution should be useful to the analysis of nanoscale quantum-wire structures where large strain and electric fields could be induced by the misfit strain.

Keywords: Electromechanical coupling; Anisotropic piezoelectric half-plane; Green's function; Stroh formalism; General surface boundary condition; Eshelby problem; Polygonal inclusion; Strained quantum wires

1. Introduction

The Eshelby problem (Eshelby, 1957; Willis, 1981; Mura, 1987) is of great importance in various engineering and physical fields, and is the subject of extensive studies (Bacon et al., 1978; Mura, 1987; Ting, 1996; Buryachenko, 2001). Some of the recent studies include the effective elastoplastic behavior of composites (Ju and Sun, 2001), non-uniform Gaussian and exponential eigenstrain within ellipsoids (Sharma and

* Tel.: +1-330-972-6739; fax: +1-330-972-6020.
E-mail address: pan2@uakron.edu (E. Pan).

0022-5096/$ - see front matter © 2003 Elsevier Ltd. All rights reserved.
doi:10.1016/S0022-5096(03)00120-0

Sharma, 2003), and dynamic Eshelby tensor in ellipsoidal inclusions (Michelitsch et al., 2003). While most Eshelby problems associated with isotropic elasticity have been solved analytically for both two-dimensional (2D) and three-dimensional (3D) deformations (i.e., Kouris and Mura, 1989; Downes et al., 1995; Faux et al., 1997; Glas, 2001, 2002a,b; Rodin, 1996; Markenscoff, 1993, 1998a,b; Nozaki and Taya, 2001; Yu and Sanday, 1991; Walpole, 1991; Rahman, 2001, 2002), those corresponding to anisotropic elasticity are usually solved numerically (see, e.g., Dong et al., 2003), with the exception of transversely isotropic elasticity for which an analytical solution can be derived (Rahman, 1999a,b; Withers, 1989; Yu et al., 1994).

In recent years, Eshelby problems with any shaped inclusion have been found to be particularly useful in the study of strained semiconductor quantum devices where the strain-induced quantum dot (QD) and quantum wire (QWR) growth is crucial in semiconductor nanostructure design (see, e.g., Andreev et al., 1999; Davies, 1998; Davies and Larkin, 1994; Faux and Pearson, 2000; Faux et al., 1996, 1997; Freund, 2000; Freund and Gosling, 1995; Gosling and Willis, 1995; Larkin et al., 1997; Park and Chuang, 1998; Pearson and Faux, 2000). It is further noticed recently that piezoelectric coupling could have an important contribution to the electronic and optical properties of the semiconductor structure, due to the fact that most semiconductor materials are piezoelectric, in particular, some of them are strongly electromechanically coupled (Pan, 2002a,b).

Owing to the complicated electromechanical coupling, however, only a few types of Eshelby problems have been solved so far for fully coupled piezoelectric solids. These include the ellipsoidal inclusion in transversely isotropic and piezoelectric 3D spaces (Wang, 1992; Dunn and Taya, 1993; Dunn and Wienecke, 1997; Kogan et al., 1996) and elliptical inclusion in general anisotropic piezoelectric 2D planes (Ting, 1996; Chung and Ting, 1996; Lu and Williams, 1998; Ru, 1999, 2000; Wang and Shen, 2003).

In spite of the importance of material anisotropy and electromechanical coupling in nanoscale QWR semiconductor structures, analytical solutions were obtained only for isotropic elastic full- and half-planes if the QWR has an arbitrary shape (see, e.g., Rodin, 1996; Downes et al., 1995; Faux et al., 1996, 1997; Nozaki and Taya, 1997; Nozaki et al., 2001; Kawashita and Nozaki, 2001; Glas, 2001, 2002a,b, 2003). Recently, however, Ru (1999, 2000) derived the solution due to an arbitrarily shaped inclusion in anisotropic full- and half-planes of elasticity and piezoelectricity using the special conformal mapping method. While the mathematical approach of Ru (1999, 2000) is elegant, numerical implementation might not be a trivial task. It is also noticed that truncation could be required if the conformal mapping function involves infinite terms. Therefore, it is most desirable if an exact closed-form solution can be derived for this complicated Eshelby problem.

In this paper, we thus present the exact closed-form solution for an arbitrarily shaped polygonal inclusion in anisotropic piezoelectric full- and half-planes, with the half-plane being under general surface conditions. We first express the induced elastic and piezoelectric fields in terms of a line integral on the boundary of the inclusion based on the equivalent body-force concept of eigenstrain, with the integrand being the line-source Green's function. We then carry out the line integral analytically assuming that the

inclusion is a polygon. The most remarkable feature is that the final exact closed-form solution involves only elementary functions, similar to the corresponding isotropic elastic solution (Faux et al., 1996, 1997; Nozaki and Taya, 1997; Glas, 2002a). Using the present simple solution, the elastic and piezoelectric fields due to multiple inclusions or an array of QWRs can be easily obtained by adding all the QWRs' contributions together. Furthermore, the solution to an elliptical inclusion can also be obtained by approximating the curved boundary of the inclusion with piecewise straight-line segments. As a numerical example, our solution is applied to a square-shaped quantum wire within GaAs full- and half-planes. The numerical results clearly show the importance of material orientation and piezoelectric coupling. It is further observed that the boundary condition on the surface of the half-plane can also have a great effect on the induced fields. Therefore, these results can serve as benchmarks and should be of interest to the analysis of nanoscale quantum-wire structures.

This paper is organized as follows: In Section 2, the equivalent body force of the eigenstrain is defined along with the governing equations. In Section 3, the boundary integral expression is obtained in terms of the line-source or point-source Green's function. It is remarked that results in Sections 2 and 3 are applicable to both 2D and 3D deformations. While in Section 4 the exact closed-form Green's functions in both full- and half-planes are briefly reviewed for the sake of easy reference, which include various surface boundary conditions, the exact closed-form expression for the induced elastic and electric fields due to an inclusion of arbitrary polygon is derived in Section 5. Numerical examples are presented in Section 6, and certain conclusions are drawn in Section 7.

2. Equivalent body force of eigenstrain

Let us assume that there is an extended general eigenstrain $\gamma^*_{Ij}(\gamma^*_{ij}\ \&\ -E^*_j)$ within the domain V bounded by the surface ∂V (See Fig. 1 for 2D illustration). Our task is to find the equivalent body force of this eigenstrain in V. To ease our discussion, we first define the extended strain

$$\gamma_{Ij} = \begin{cases} \gamma_{ij}, & I = i = 1,2,3, \\ -E_j, & I = 4, \end{cases} \tag{1}$$

where γ_{ij} is the total elastic strain and E_j is the total electric field, which are related to the total elastic displacement u_i and the total electric potential ϕ as

$$\gamma_{ij} = 0.5(u_{i,j} + u_{j,i}),$$
$$E_j = -\phi_{,j}. \tag{2}$$

It is further noted that the total extended strain can be written as

$$\gamma_{Ij} = \gamma^{\mathrm{e}}_{Ij} + \gamma^*_{Ij}, \tag{3}$$

where γ^*_{Ij} is the extended eigenstrain in the inclusion (Fig. 1), and γ^{e}_{Ij} is the extended strain that appears in the constitutive relation (Barnett and Lothe, 1975;

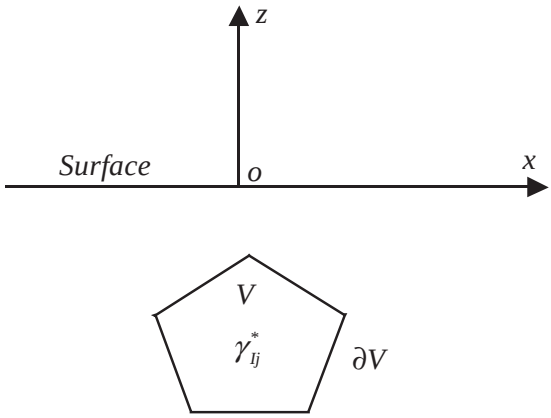

Fig. 1. A general inclusion problem in an anisotropic piezoelectric (x,z)-half-plane ($z<0$): An extended eigenstrain $\gamma^*_{Ij}(\gamma^*_{ij}\ \&\ -E^*_j)$ within an arbitrarily shaped polygon.

Dunn and Taya, 1993; Pan, 1999) as

$$\sigma_{iJ} = C_{iJKl}\gamma^{e}_{Kl} \tag{4a}$$

or

$$\sigma_{iJ} = C_{iJKl}(\gamma_{Kl} - \chi\gamma^*_{Kl}). \tag{4b}$$

In Eq. (4), χ is equal to 1 if the field point is within the eigenstrain domain V and to 0 otherwise. The extended stress in Eq. (4) is defined by

$$\sigma_{iJ} = \begin{cases} \sigma_{ij}, & J = j = 1,2,3, \\ D_i, & J = 4, \end{cases} \tag{5}$$

where σ_{ij} and D_i are the stress and electric displacement, respectively, and

$$C_{iJKl} = \begin{cases} C_{ijkl}, & J,K = j,k = 1,2,3, \\ e_{lij}, & J = j = 1,2,3;\ K = 4, \\ e_{ikl}, & J = 4;\ K = k = 1,2,3, \\ -\varepsilon_{il}, & J = K = 4 \end{cases} \tag{6}$$

with C_{ijkl}, e_{lij} and ε_{il} being the elastic moduli, piezoelectric coefficients, and dielectric constants, respectively (Tiersten, 1969; Suo et al., 1992). When $e_{lij} = 0$, the solution derived in this paper is then reduced to the one corresponding to the Eshelby problem in anisotropic elastic full- and half-planes.

In this paper, we further define the extended displacement

$$u_I = \begin{cases} u_i, & I = i = 1,2,3, \\ \phi, & I = 4. \end{cases} \tag{7}$$

For the eigenstrain problem, the equilibrium equation for the stresses and the balance for the electric displacements are (Tiersten, 1969; Pan, 1999)

$$\sigma_{iJ,i} = 0 \tag{8}$$

Now, for the extended eigenstrain γ^*_{Ij} in the inclusion V, substitution of Eq. (4b) into Eq. (8) gives

$$C_{iJKl} u_{K,li} = C_{iJKl} \gamma^*_{Kl,i}. \tag{9}$$

It is clear that the right-hand side of Eq. (9) resembles the extended body force as would appear on the left-hand side of Eq. (8), i.e.,

$$f_J = -C_{iJKl} \gamma^*_{Kl,i} \tag{10}$$

which is the equivalent body force of the eigenstrain. This concept is an extension of the purely elastic counterpart (Mura, 1987) to the piezoelectric solid. The equivalent body force will be employed in the next section to find the induced total extended displacement u_I and total extended strain γ_{Ij}.

3. Boundary integral expression in terms of Green's function

For the extended general eigenstrain γ^*_{Ij} at $\boldsymbol{x} = (x, y, z)$ within the domain V, the induced extended displacement at $\boldsymbol{X} = (X, Y, Z)$ can be found using the superposition method. In other words, the response is an integral, over V, of the equivalent body force defined by Eq. (10), multiplied by the point-source (line-source for 2D) Green's function, i.e.,

$$u_K(\boldsymbol{X}) = -\int_V u^K_J(\boldsymbol{x}; \boldsymbol{X}) [C_{iJLm} \gamma^*_{Lm}(\boldsymbol{x})]_{,i} \, \mathrm{d}V(\boldsymbol{x}), \tag{11}$$

where $u^K_J(\boldsymbol{x}; \boldsymbol{X})$ is the Jth Green's elastic displacement/electric potential at $\boldsymbol{x}$ due to a point-force/point-charge in the Kth direction applied at $\boldsymbol{X}$. This again extends the purely elastic expression (Mura, 1987; Faux et al., 1997; Nozaki and Taya, 1997; Glas, 2003) to the piezoelectric one.

Integrating by parts and noticing that the eigenstrain is nonzero only in V, Eq. (11) can be written alternatively as

$$u_K(\boldsymbol{X}) = \int_V u^K_{J,x_i}(\boldsymbol{x}; \boldsymbol{X}) C_{iJLm} \gamma^*_{Lm}(\boldsymbol{x}) \, \mathrm{d}V(\boldsymbol{x}). \tag{12}$$

If we further assume that the eigenstrain is uniform within the domain V, then the domain-integral in Eq. (12) can be transformed into the boundary of V. That is

$$u_K(\boldsymbol{X}) = C_{iJLm} \gamma^*_{Lm} \int_{\partial V} u^K_J(\boldsymbol{x}; \boldsymbol{X}) n_i(\boldsymbol{x}) \, \mathrm{d}S(\boldsymbol{x}), \tag{13}$$

where $n_i(\boldsymbol{x})$ is the outward normal on the boundary ∂V.

To find the elastic strain and electric fields, we take the derivatives of Eq. (13) with respect to the field point $\boldsymbol{X}$ (i.e., the source point of the point-force/point-charge

Green's function), which yields

$$\gamma_{kp}(\boldsymbol{X}) = \frac{1}{2}\,\gamma^*_{Lm} C_{iJLm} \int_{\partial V} [u^k_{J,X_p}(\boldsymbol{x};\boldsymbol{X}) + u^p_{J,X_k}(\boldsymbol{x};\boldsymbol{X})] n_i(\boldsymbol{x})\,\mathrm{d}S(\boldsymbol{x});$$

$$k, p = 1,2,3, \tag{14a}$$

$$E_p(\boldsymbol{X}) = -\gamma^*_{Lm} C_{iJLm} \int_{\partial V} u^4_{J,X_p}(\boldsymbol{x};\boldsymbol{X}) n_i(\boldsymbol{x})\,\mathrm{d}S(\boldsymbol{x}); \qquad p = 1,2,3. \tag{14b}$$

The stresses and electric displacements are obtained from Eq. (4b).

We remark that the results presented in this and previous sections can be applied to both 2D and 3D inclusion problems. In particular, Eqs. (13) and (14) are very useful, since for a uniform eigenstrain within a homogeneous piezoelectric solid, the elastic and piezoelectric fields can be obtained by performing an integral over the boundary of the inclusion, using the available piezoelectric Green's function (see, e.g., Pan, 2002c) as the integrand. However, instead of numerically carrying out the boundary integrals in Eqs. (13) and (14), we will show in Section 5 that for an arbitrary polygonal inclusion within a piezoelectric half-plane (with the full-plane being the special case), the induced elastic and piezoelectric fields can be derived in an exact closed form. Such an exact closed-form solution is unavailable to the best of the author's knowledge, except for the corresponding isotropic elastic full- (Rodin, 1996; Faux et al., 1996, 1997; Nozaki and Taya, 1997) and half-plane (Glas, 2002a,b) cases. To facilitate our discussion, we first briefly review the Green's functions in full- and half-planes based on the extended Stroh formalism. For a detailed derivation on these Green's functions, one is referred to, for example, Pan (2002c) and the references therein.

4. Piezoelectric half-plane Green's function

We consider an anisotropic piezoelectric half-plane with its surface at $z = 0$ and the half-plane can occupy either the $z > 0$ or $z < 0$ domain. We assume that the deformation is independent of the y-coordinate (i.e., the generalized plane strain deformation in the (x,z) plane). It is emphasized that we use the (x,z) plane, instead of the common (x,y) plane. The reason is that under the (x,z) plane, the Stroh formalism is consistent with that in 3D, and that various boundary conditions on the surface of the half-plane can be handled uniformly (Pan, 2002c). We further let an extended line force $\boldsymbol{f} = (f_1, f_2, f_3, -q)$ be applied at (X,Z) with $Z > 0$ or $Z < 0$, depending upon the half-plane one chooses. The subscripts 1, 2, and 3 denote the x-, y-, and z-directions, respectively.

It can be shown that (Ting, 1996; Pan, 2002c) the half-plane Green's functions (i.e., the extended displacement vector $\boldsymbol{u}$ and stress function vector $\boldsymbol{\psi}$) can be expressed as

$$\boldsymbol{u} = \frac{1}{\pi}\,\mathrm{Im}\{\boldsymbol{A}\langle \ln(z_* - s_*)\rangle \boldsymbol{q}^\infty\} + \frac{1}{\pi}\,\mathrm{Im}\sum_{J=1}^{4}\{\boldsymbol{A}\langle \ln(z_* - \bar{s}_J)\rangle \boldsymbol{q}_J\}, \tag{15a}$$

$$\boldsymbol{\psi} = \frac{1}{\pi}\,\mathrm{Im}\{\boldsymbol{B}\langle \ln(z_* - s_*)\rangle \boldsymbol{q}^\infty\} + \frac{1}{\pi}\,\mathrm{Im}\sum_{J=1}^{4}\{\boldsymbol{B}\langle \ln(z_* - \bar{s}_J)\rangle \boldsymbol{q}_J\}, \tag{15b}$$

where the extended stress function vector $\boldsymbol{\psi}$ (a four-dimensional vector) is related to the elastic stresses and electrical displacements through

$$\sigma_{1J} = -\psi_{J,3}; \quad \sigma_{3J} = \psi_{J,1}. \tag{16}$$

Also in Eq. (15), an over bar stands for the complex conjugate, Im for the imaginary part of a complex variable, and p_J, $\boldsymbol{A}$, and $\boldsymbol{B}$ denote the Stroh eigenvalues and the corresponding eigenmatrices with their expressions given in Appendix A. Finally in Eq. (15),

$$\langle \ln(z_* - s_*) \rangle = \mathrm{diag}[\ln(z_1 - s_1), \ln(z_2 - s_2), \ln(z_3 - s_3), \ln(z_4 - s_4)],$$

$$\langle \ln(z_* - \bar{s}_J) \rangle = \mathrm{diag}[\ln(z_1 - \bar{s}_J), \ln(z_2 - \bar{s}_J), \ln(z_3 - \bar{s}_J), \ln(z_4 - \bar{s}_J)], \tag{17}$$

where the complex variables z_J and s_J are defined, respectively, by

$$z_J = x + p_J z, \tag{18a}$$

$$s_J = X + p_J Z. \tag{18b}$$

It is further noticed that the first term in Eq. (15) corresponds to the full-plane Green's function with

$$\boldsymbol{q}^{\infty} = \boldsymbol{A}^{\mathrm{T}} \boldsymbol{f}, \tag{19}$$

where the superscript T denotes the matrix transpose.

The second term in Eq. (15) is the complementary part of the solution with the complex constant vectors $\boldsymbol{q}_J (J = 1, 2, 3, 4)$ to be determined. For the 16 sets of the surface boundary conditions discussed in Pan (2002c), we define a 4×4 complex matrix $\boldsymbol{K}$ as

$$\mathbf{K} = \mathbf{I}_u \mathbf{A} + \mathbf{I}_t \mathbf{B}, \tag{20}$$

where $\boldsymbol{I}_u$ and $\boldsymbol{I}_t$ are 4×4 diagonal matrices whose four diagonal elements are either one or zero, and satisfy conditions

$$\mathbf{I}_u + \mathbf{I}_t = \mathbf{I}; \quad \mathbf{I}_u \mathbf{I}_t = \mathbf{0}. \tag{21}$$

with $\boldsymbol{I}$ being the identity matrix. With this newly defined complex matrix $\boldsymbol{K}$, the involved complex constants in Eq. (15) can be found, in a remarkably simple and unified form, as

$$\boldsymbol{q}_J = \boldsymbol{K}^{-1} \bar{\boldsymbol{K}} \boldsymbol{I}_J \bar{\boldsymbol{q}}^{\infty}, \tag{22}$$

where the diagonal matrices $\boldsymbol{I}_J$ have the following diagonal elements

$$\boldsymbol{I}_1 = \mathrm{diag}[1, 0, 0, 0]; \quad \boldsymbol{I}_2 = \mathrm{diag}[0, 1, 0, 0]$$

$$\boldsymbol{I}_3 = \mathrm{diag}[0, 0, 1, 0]; \quad \boldsymbol{I}_4 = \mathrm{diag}[0, 0, 0, 1] \tag{23}$$

Thus, the extended displacement and stress function vectors due to an extended line force $\boldsymbol{f} = (f_1, f_2, f_3, -q)$ in a generally anisotropic and piezoelectric half-plane with the 16 different sets of surface boundary conditions are all derived in a very concise form.

With the extended displacement and stress function vectors given by Eq. (15), their derivatives with respect to the field and source points can be analytically carried out and the resulting Green's functions can then be applied to various problems associated with a half-plane under general boundary conditions. In the following section, however, we derive the exact boundary integral for these Green's functions by assuming that the boundary of the inclusion is made of piecewise straight-line segments.

5. Analytical integral of a straight-line segment

To carry out the line integral in Eqs. (13) and (14), we first write the Green's displacement in Eq. (15) in a matrix form the same way as in Eq. (13). That is,

$$u_J^K(\boldsymbol{x},\boldsymbol{X}) = \frac{1}{\pi}\,\mathrm{Im}\{A_{JR}\ln(z_R - s_R)A_{KR}\} + \frac{1}{\pi}\mathrm{Im}\sum_{v=1}^{4}\{A_{JR}\ln(z_R - \bar{s}_v)Q_{RK}^v\}, \tag{24}$$

where the index K again is for the four line-source directions ($K = k = 1,2,3$ for the line force, and $K = 4$ for the negative line charge). Also in Eq. (24),

$$Q_{RN}^v = K_{RS}^{-1}\bar{K}_{SP}(I_v)_P\bar{A}_{NP}. \tag{25}$$

Define a line segment in the (x,z)-plane starting from point 1 (x_1,z_1) and ending at point 2 (x_2,z_2), in terms of the parameter t $(0 \leqslant t \leqslant 1)$, as

$$x = x_1 + (x_2 - x_1)t,$$

$$z = z_1 + (z_2 - z_1)t. \tag{26}$$

Then, the outward normal component $n_i(\boldsymbol{x})$ along the line segment is constant, given by

$$n_1 = (z_2 - z_1)/l; \quad n_2 = -(x_2 - x_1)/l, \tag{27}$$

where $l = \sqrt{(x_2 - x_1)^2 + (z_2 - z_1)^2}$ is the length of the line segment. It is obvious that the elemental length is $\mathrm{d}S = l\,\mathrm{d}t$.

It is noted that the half-plane Green's functions consist of two parts: the full-plane Green's function and a complementary part. Therefore, the corresponding integrals also consist of two parts involving two types of functions. For the first integral, we define

$$h_R(X,Z) \equiv \int_0^1 \ln(z_R - s_R)\,\mathrm{d}t \tag{28}$$

or

$$h_R(X,Z) = \int_0^1 \ln\{[(x_2 - x_1) + p_R(z_2 - z_1)]t + [(x_1 + p_R z_1) - s_R]\}\,\mathrm{d}t. \tag{29}$$

Integration of this expression gives

$$h_R(X,Z) = \frac{(x_1 + p_R z_1) - s_R}{(x_2 - x_1) + p_R(z_2 - z_1)}\ln\left[\frac{x_2 + p_R z_2 - s_R}{x_1 + p_R z_1 - s_R}\right] + \ln[x_2 + p_R z_2 - s_R] - 1. \tag{30}$$

Similarly, we define the second integral as

$$g_R^v(X,Z) \equiv \int_0^1 \ln(z_R - \bar{s}_v)\,\mathrm{d}t \tag{31}$$

and the integration of the right-hand side gives

$$g_R^v(X,Z) = \frac{(x_1 + p_R z_1) - \bar{s}_v}{(x_2 - x_1) + p_R(z_2 - z_1)} \ln\left[\frac{x_2 + p_R z_2 - \bar{s}_v}{x_1 + p_R z_1 - \bar{s}_v}\right] + \ln[x_2 + p_R z_2 - \bar{s}_v] - 1. \tag{32}$$

Therefore, the induced elastic displacements and piezoelectric potential, due to the contribution of a straight-line segment along the boundary of the inclusion, can be obtained in the following exact closed form:

$$u_K(\boldsymbol{X}) = n_i C_{iJLm}\gamma_{Lm}^* \frac{l}{\pi}\,\mathrm{Im}\left\{A_{JR}h_R(X,Z)A_{KR} + \sum_{v=1}^{4} A_{JR}g_R^v(X,Z)Q_{RK}^v\right\}. \tag{33}$$

Notice that the first term involving h_R is the contribution from the full-plane Green's function, and the second term involving g_R^v comes from the complementary part, which is used to satisfy the boundary conditions on the surface of the half-plane. Therefore, Eq. (33) contains the solution for the inclusion problems in both full- and half-planes. By adding contributions from all line segments of the boundary, the solution to an inclusion with a general polygonal shape in either a full- or a half-plane is then obtained in an exact closed form!

The exact closed-form strain and electric field can be obtained either by carrying out the integral as we have just done for the elastic displacement and electric potential, or by simply taking the derivative of Eq. (33) with respect to the coordinate $\boldsymbol{X} = (X, Z)$. By following the second approach, we obtain the elastic strain and electric field, due to a straight-line segment of the boundary of the inclusion, as ($\alpha, \beta = 1$ and 3)

$$\gamma_{\beta\alpha}(\boldsymbol{X}) = 0.5 n_i C_{iJLm}\gamma_{Lm}^* \frac{l}{\pi}\mathrm{Im}\left\{A_{JR}h_{R,\alpha}(X,Z)A_{\beta R} + \sum_{v=1}^{4} A_{JR}g_{R,\alpha}^v(X,Z)Q_{R\beta}^v\right\} + 0.5 n_i C_{iJLm}\gamma_{Lm}^* \frac{l}{\pi}\,\mathrm{Im}\left\{A_{JR}h_{R,\beta}(X,Z)A_{\alpha R} + \sum_{v=1}^{4} A_{JR}g_{R,\beta}^v(X,Z)Q_{R\alpha}^v\right\}, \tag{34}$$

$$\gamma_{2\alpha}(\boldsymbol{X}) = 0.5 n_i C_{iJLm}\gamma_{Lm}^* \frac{l}{\pi}\,\mathrm{Im}\left\{A_{JR}h_{R,\alpha}(X,Z)A_{2R} + \sum_{v=1}^{4} A_{JR}g_{R,\alpha}^v(X,Z)Q_{R2}^v\right\}, \tag{35}$$

$$E_\alpha(\boldsymbol{X}) = -n_i C_{iJLm}\gamma_{Lm}^* \frac{l}{\pi}\,\mathrm{Im}\left\{A_{JR}h_{R,\alpha}(X,Z)A_{4R} + \sum_{v=1}^{4} A_{JR}g_{R,\alpha}^v(X,Z)Q_{R4}^v\right\}, \tag{36}$$

where

$$h_{R,1}(X,Z)=\frac{-1}{(x_2-x_1)+p_R(z_2-z_1)}\ln\left[\frac{x_2+p_Rz_2-s_R}{x_1+p_Rz_1-s_R}\right], \tag{37}$$

$$h_{R,3}(X,Z)=\frac{-p_R}{(x_2-x_1)+p_R(z_2-z_1)}\ln\left[\frac{x_2+p_Rz_2-s_R}{x_1+p_Rz_1-s_R}\right], \tag{38}$$

$$g^v_{R,1}(X,Z)=\frac{-1}{(x_2-x_1)+p_R(z_2-z_1)}\ln\left[\frac{x_2+p_Rz_2-\bar{s}_v}{x_1+p_Rz_1-\bar{s}_v}\right], \tag{39}$$

$$g^v_{R,3}(X,Z)=\frac{-\bar{p}_v}{(x_2-x_1)+p_R(z_2-z_1)}\ln\left[\frac{x_2+p_Rz_2-\bar{s}_v}{x_1+p_Rz_1-\bar{s}_v}\right]. \tag{40}$$

With these strain and electric fields, the stresses and electric displacements are then found from Eq. (4b).

It is observed from Eqs. (30)–(33) that the elastic displacement and electric potential are continuous everywhere including all the corners of the polygon or the vertexes. From Eqs. (34)–(40), however, we notice that at the vertices, some of the strain and electric field components may exhibit a logarithmic singularity for the terms corresponding to the full-plane solution (i.e., in Eqs. (37) and (38) when $s_R = x_1 + p_Rz_1$ or $s_R = x_2 + p_Rz_2$). For a polygonal inclusion in an isotropic elastic full-plane, Rodin (1996) discussed the vertex singularity of the Eshelby tensor in general, whilst Downes et al. (1995) and Nozaki et al. (2001) showed that this singularity was only associated with the shear stress/strain component in their examples. For the square QWR cases studied in this paper, we found that if the full- or half-plane is GaAs (001) (defined below), then only the shear strain component γ_{xz} (and its corresponding shear stress component) is logarithmically singular at the four corners. However, if the full- or half-plane is GaAs (111) (again, defined below), then all the strain and electric field components are logarithmically singular at the four corners. Therefore, in the numerical calculation presented below, the corners are avoided by slightly perturbing their exact coordinates (e.g., replacing $(x,z)=(10\text{ nm}, 10\text{ nm})$ with $(x,z)=(9.99\text{ nm}, 9.99\text{ nm})$), just like Downes et al. (1995) and Rodin (1996) did in their strain analysis in polygons within the isotropic elastic full-plane.

We further remark that Eqs. (34)–(36) can be expressed alternatively using the extended Eshebly tensor S (Eshelby, 1961; Mura, 1987; Dunn and Taya, 1993; Dunn and Wienecke, 1997), as

$$\gamma_{Ij}=S_{IjLm}\gamma^*_{Lm}, \tag{41}$$

where the elements of the extended Eshebly tensor S are readily obtained by comparing Eq. (41) to Eqs. (34)–(36). Furthermore, the total extended Eshelby tensor in Eq. (41) can be expressed as a sum of two other tensors, i.e.,

$$S_{IjLm}=S^{\infty}_{IjLm}+S^{c}_{IjLm}, \tag{42}$$

where the first term is the Eshelby tensor in anisotropic piezoelectric full-plane, and the second is the complementary term introduced to satisfy the boundary condition on the surface of the half-plane.

Table 1
Induced dimensionless stress component $\bar{\sigma}_{xx}$ within the elliptical inclusion

$X = Z$ (nm)	$N = 10$	$N = 25$	$N = 50$	$N = 100$
0	−0.0380101	−0.0379582	−0.0379582	−0.0379582
1	−0.0380030	−0.0379580	−0.0379582	−0.0379582
2	−0.0379792	−0.0379578	−0.0379582	−0.0379582
3	−0.0379304	−0.0379587	−0.0379582	−0.0379582
4	−0.0378358	−0.0379608	−0.0379582	−0.0379582
5	−0.0376532	−0.0379581	−0.0379583	−0.0379582
6	−0.0373154	−0.0379453	−0.0379579	−0.0379582
7	−0.0367980	−0.0379681	−0.0379597	−0.0379583
8	−0.0361470	−0.0381939	−0.0379390	−0.0379594

In summary, therefore, we have derived the exact closed-form solutions for the elastic and piezoelectric fields induced by an arbitrary polygonal inclusion. Since our result is in an exact closed form, solution to multiple inclusions can be simply derived by superposing the contributions from all inclusions. This is particularly useful in the analysis of QWR-array induced elastic and piezoelectric fields (Glas, 2002a, b). Furthermore, a solution to the inclusion with curved boundary can also be obtained by approximating the curved boundary with piecewise straight-line segments.

6. Numerical examples

Before applying our exact closed-form solutions to a buried QWR in the piezoelectric GaAs, we have first checked these solutions with available results for a rectangular QWR in an isotropic elastic full-plane (Downes et al., 1995) and a trapezoidal QWR in an isotropic elastic half-plane (Glas, 2002a). We have also compared our results for a N-sided regular polygon in an isotropic elastic full-plane for $N = 3$, 6, and 12 (Rodin, 1996). We found that our solutions are the same as these previously published exact results.

Another interesting verification for the present solutions is to use the well-known fact (Eshelby, 1961; Mura, 1987; Rodin, 1996; Ru, 2000) that the stress and electric displacement fields within an elliptical inclusion in a full-plane are constants. We assume an elliptical inclusion with major axis along the x-direction and minor axis along the z-direction. The semi-major and semi-minor axes are, respectively, $a = 20$ nm and $b = 10$ nm. The eigenstrain is assumed to be hydrostatic, i.e., $\gamma^*_{xx} = \gamma^*_{zz} = 0.07$ and the full-plane is GaAs (111) with its material properties being discussed below. To use our exact closed-form solutions, we replace the curved ellipse with N piecewise straight-line segments, i.e., replacing the ellipse with a N-sided regular polygon. For N equals 10, 25, 50, and 100, the results for the dimensionless stress component $\bar{\sigma}_{xx}(=\sigma_{xx}/(0.154 \times 10^{12})$ and electric displacement component $\bar{d}_x(=d_x/0.18475209)$ are given, respectively, in Tables 1 and 2 for selected internal points. It is clear from these two tables that they are indeed constants within the elliptical inclusion when N

Table 2
Induced dimensionless electric displacement component $\bar{d}_x$ within the elliptical inclusion

$X = Z$ (nm)	$N = 10$	$N = 25$	$N = 50$	$N = 100$
0	−0.0205255	−0.0206011	−0.0206011	−0.0206011
1	−0.0204898	−0.0206004	−0.0206011	−0.0206011
2	−0.0203928	−0.0206031	−0.0206011	−0.0206011
3	−0.0202605	−0.0206058	−0.0206011	−0.0206011
4	−0.0201246	−0.0205942	−0.0206012	−0.0206011
5	−0.0200136	−0.0205715	−0.0206011	−0.0206011
6	−0.0199524	−0.0206142	−0.0206006	−0.0206011
7	−0.0196873	−0.0208139	−0.0206086	−0.0206010
8	−0.0172762	−0.0207988	−0.0204821	−0.0205961

is equal to or larger than 50. It is further noticed that for points near the center, the stress and electric displacement reach the final constant values even for small N (i.e., $N = 25$); However, for points close to the boundary, i.e., point $X = Z = 8$ nm, the convergence is slow. We have also checked other stresses and electric displacements due to different eigenstrain components, and found that they all converge to constants for large N (i.e., $N = 100$).

We now apply the exact closed-form solutions, i.e., Eqs. (33)–(36), to a square QWR in piezoelectric GaAs. The QWR has a dimension of 20 nm × 20 nm, and for the half-plane case, is located symmetrically (about the z-axis) below the surface at a depth 5 nm. The misfit-strain is again hydrostatic, i.e., $\gamma^*_{xx} = \gamma^*_{zz} = 0.07$. The elastic properties for GaAs are $C_{11} = 118 \times 10^9$ N/m^2, $C_{12} = 54 \times 10^9$ N/m^2, and $C_{44} = 59 \times 10^9$ N/m^2 (Pan, 2002b). The piezoelectric constant and relative permeability for GaAs (001) are, respectively, $e_{14} = -0.16$ C/m^2 and $\varepsilon_r = 12.5$ (Pan, 2002b). For GaAs (001), the global coordinates x, y, and z are coincident with the crystalline axes [100], [010], and [001]. For GaAs (111), the x-axis is along [11 − 2], y-axis along [− 110], and z-axis along [111] directions of the crystalline (Pan, 2002b). For the half-plane problem, two cases of boundary conditions on the surface of the half-plane are considered: Case I for the traction-free insulating condition, and Case II for the traction-free conducting condition (Pan, 2002c).

Shown in Figs. 2a and 2b are, respectively, the contours of the strain component γ_{xx} and hydrostatic strain $\gamma_{xx} + \gamma_{zz}$ in the square QWR within the GaAs (001) full-plane. It is observed from Fig. 2a that while the two equal maximums of γ_{xx} are reached in the middle of left and right sides of the square with a value (=0.062) slightly less than the misfit-strain, the two equal minimums are reached in the middle of the top and bottom sides of the square with a value (=0.036) slightly over half of the misfit-strain. The hydrostatic strain (Fig. 2b), however, has a very gentle variation in the square QWR, with the maximum difference less than 10%. Notice further that these normal strains are finite at the four corners.

Figs. 3a and b show the corresponding contours of γ_{xx} and $\gamma_{xx} + \gamma_{zz}$ in the square QWR within the GaAs (111) full-plane. Comparing these two figures to Figs. 2a and b, we immediately observe that both the strain values and the contour shapes are

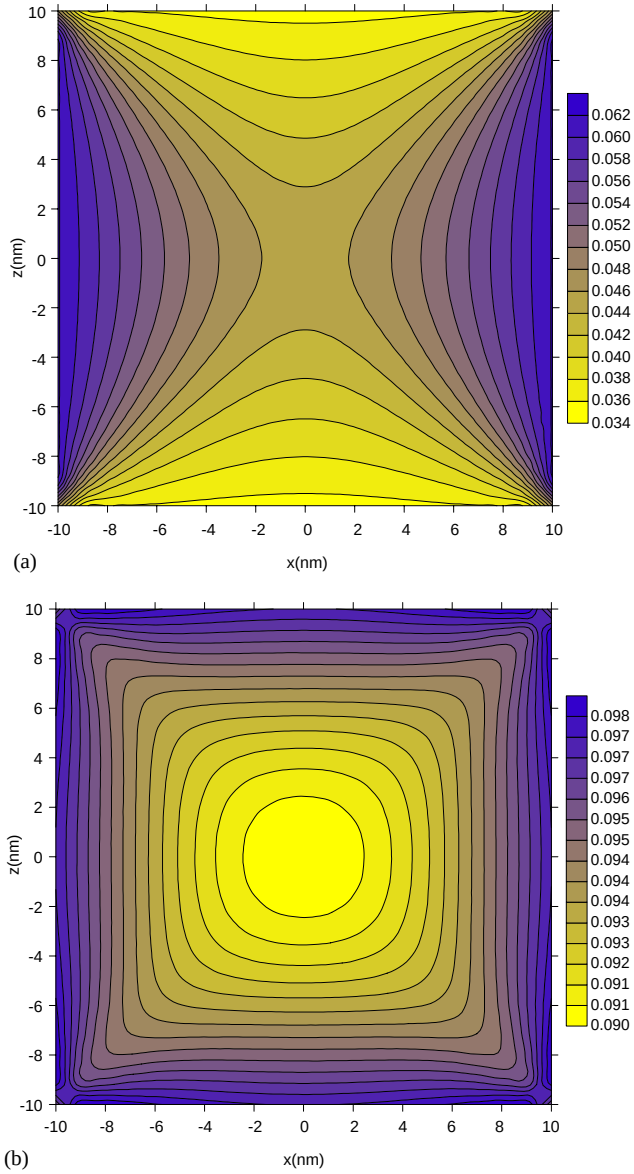

Fig. 2. Contours of strain component γ_{xx} (a) and hydrostatic strain $\gamma_{xx} + \gamma_{zz}$ (b) in a square QWR of 20 nm × 20 nm within the GaAs (001) full-plane.

very different for the two differently oriented GaAs semiconductors. In particular, since the elastic strain field in GaAs (111) is singular at the four corners (Fig. 3b for the contour concentration), one should try to avoid sharp corners when growing QWR in an inclined orientation such as the (111)-oriented.

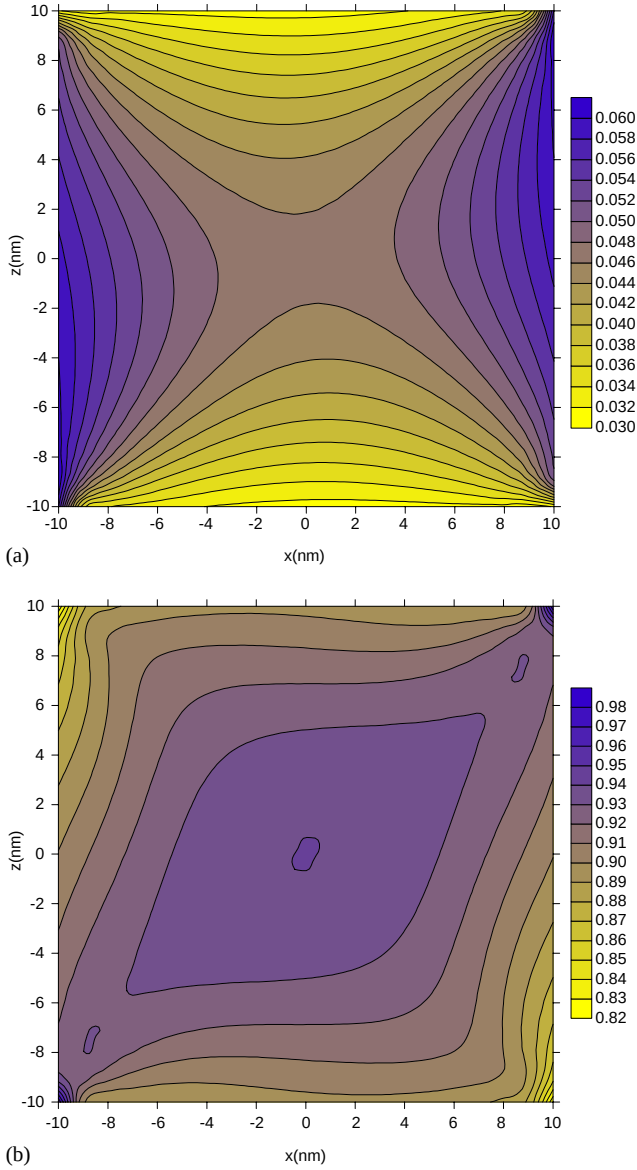

Fig. 3. Contours of strain component γ_{xx} (a) and hydrostatic strain $\gamma_{xx} + \gamma_{zz}$ (b) in a square QWR of 20 nm × 20 nm within the GaAs (111) full-plane.

While the contours of the piezoelectric potential ϕ (in V) are shown in Fig. 4, those of the electric components E_x and E_z (in V/m) are plotted, respectively, in Figs. 5a and b. It is noted that these contours are for the GaAs (111) full-plane. There is no induced piezoelectric potential and electric fields should the crystalline axes

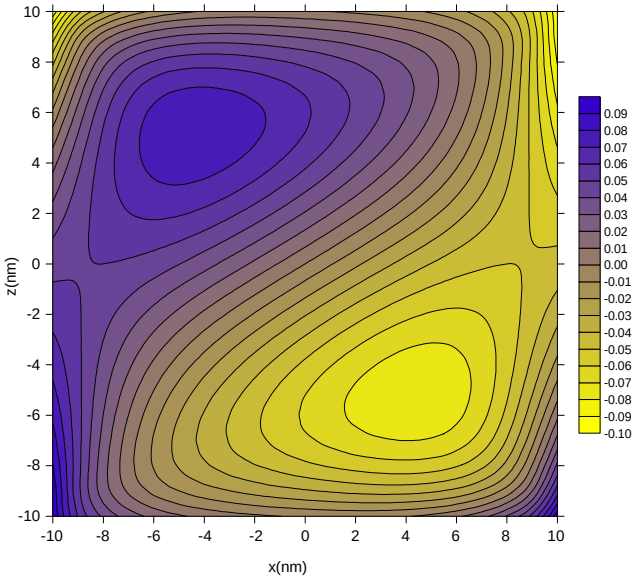

Fig. 4. Contours of piezoelectric potential ϕ (in V) in a square QWR of 20 nm $\times$ 20 nm within the GaAs (111) full-plane.

of the semiconductor GaAs be along the x-, y-, and z-axes, i.e., the semiconductor GaAs (001), no matter if it is for an inclusion in a full-plane or in a half-plane. This result is actually consistent with the previous well-known observation for the superlattice structures (Smith, 1986), but is different from our recent observation for the QD structures (Pan, 2002b) where large electric field can also be induced by the QD in the GaAs (001) substrate! Furthermore, similar to the elastic strain field in Figs. 3a and b, the electric field singularities (Figs. 5a and b) can be clearly observed at the four corners, and therefore these points could be critical in the QWR structure analysis.

The results that we have presented above are for a square-shaped QWR in a full-plane. However, a more realistic QWR structure model would be for the QWR within a half-plane, and thus the effect of traction-free surface needs to be addressed. Further consideration is also needed for the effect of different electric surface conditions. Therefore, in the following analysis, two different electric surface conditions are studied: Case I for the traction-free insulating surface condition, and Case II for the traction-free conducting surface condition. Since GaAs is a weekly coupled piezoelectric material, the induced elastic fields are nearly identical for both cases of the surface conditions (Pan, 2002a, b). Thus, only those corresponding to the Case I surface condition are presented for the elastic field.

Figs. 6a and b show the contours of the strain component γ_{xx} and hydrostatic strain $\gamma_{xx} + \gamma_{zz}$ in the square QWR. As we mentioned earlier, this square QWR is within the GaAs (001) half-plane and its topside is at a depth of 5 nm below the free surface.

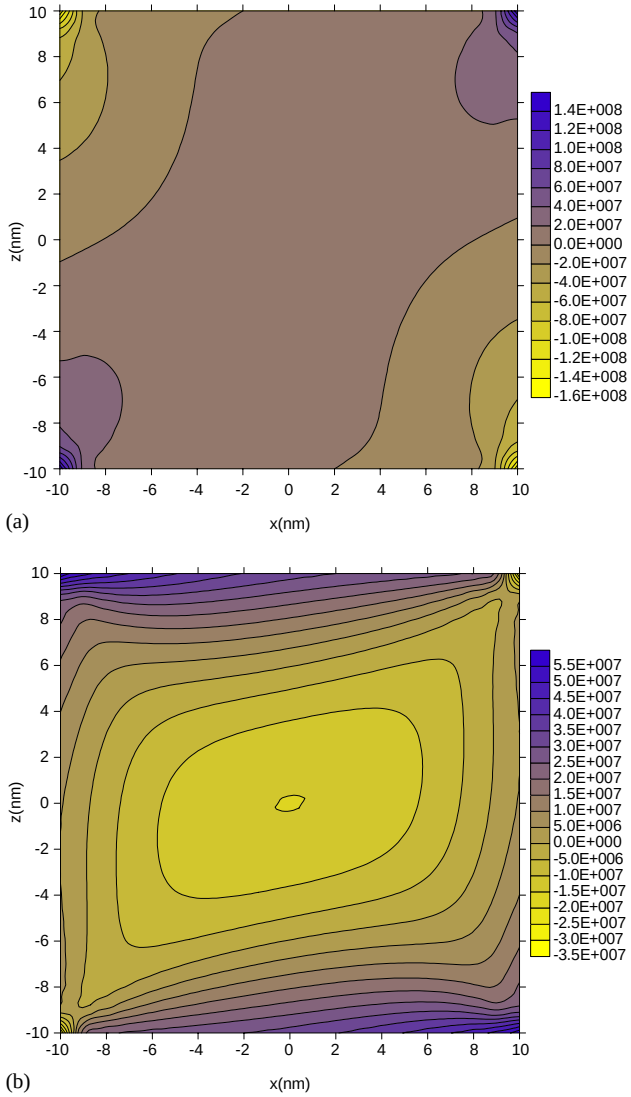

Fig. 5. Contours of electric components E_x (a) and E_z (b) (in V/m) in a square QWR of 20 nm × 20 nm within the GaAs (111) full-plane.

Comparing these two figures to those in the GaAs (001) full-plane (i.e., Figs. 2a and b), we observe that the free surface not only alters the contour shapes substantially, but also increases the magnitude of the strain field. For instance, compared to the full-plane result, the strain component γ_{xx} and the hydrostatic strain have increased, respectively, about 13% and 25% due to the effect of the free surface.

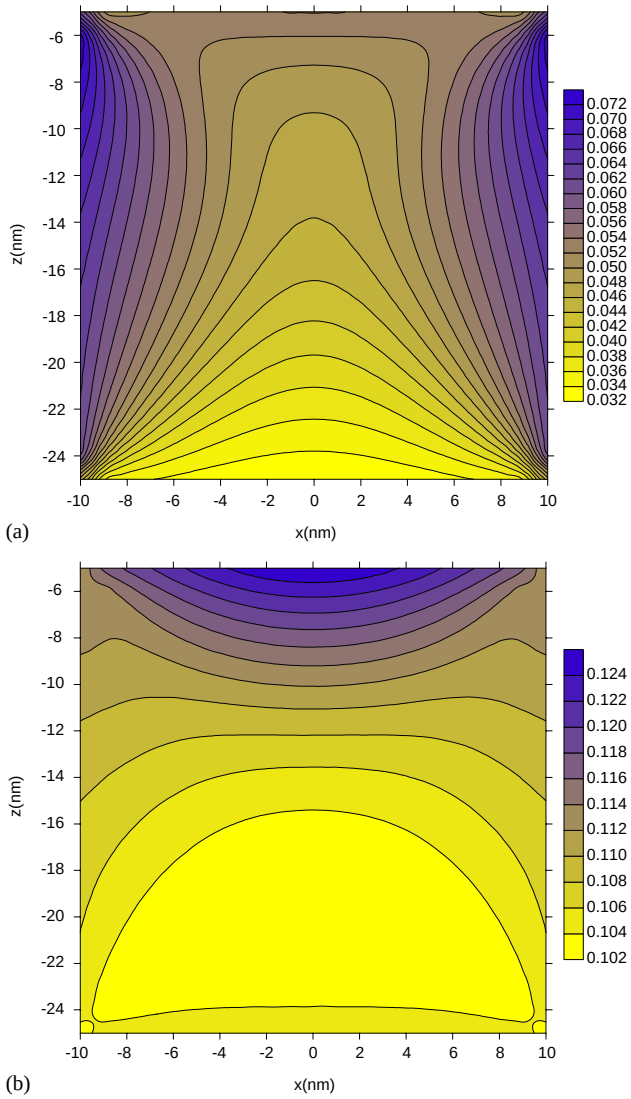

Fig. 6. Contours of strain component γ_{xx} (a) and hydrostatic strain $\gamma_{xx} + \gamma_{zz}$ (b) in a square QWR of 20 nm × 20 nm within the GaAs (001) half-plane.

Similarly, Figs. 7a and b plot the contours of the strain component γ_{xx} and hydrostatic strain $\gamma_{xx} + \gamma_{zz}$ in the square QWR within the GaAs (111) half-plane. Again, the influence of the free surface on the elastic strain distribution is clearly observed when compared these two figures to the corresponding full-plane results (Figs. 3a and b).

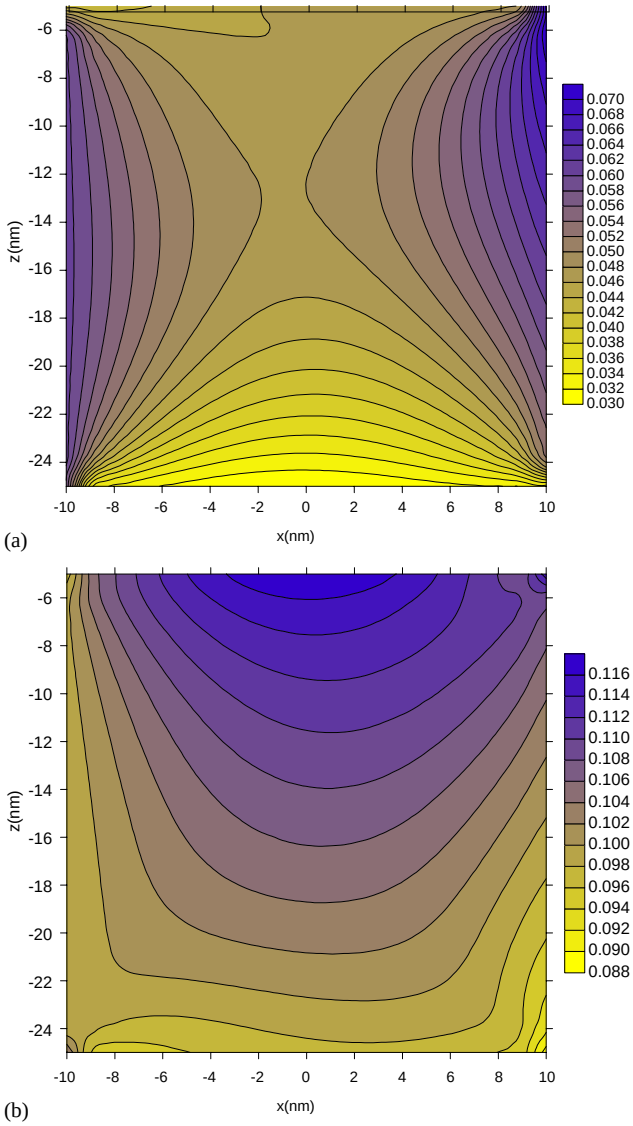

Fig. 7. Contours of strain component γ_{xx} (a) and hydrostatic strain $\gamma_{xx}+\gamma_{zz}$ (b) in a square QWR of 20 nm × 20 nm within the GaAs (111) half-plane.

Although different electric surface conditions result in nearly identical elastic field in GaAs, they can cause totally different piezoelectric fields. For example, Figs. 8a and b show the contours of the piezoelectric potential ϕ (in V), respectively, corresponding to the boundary condition Cases I and II in the square QWR within the GaAs (111)

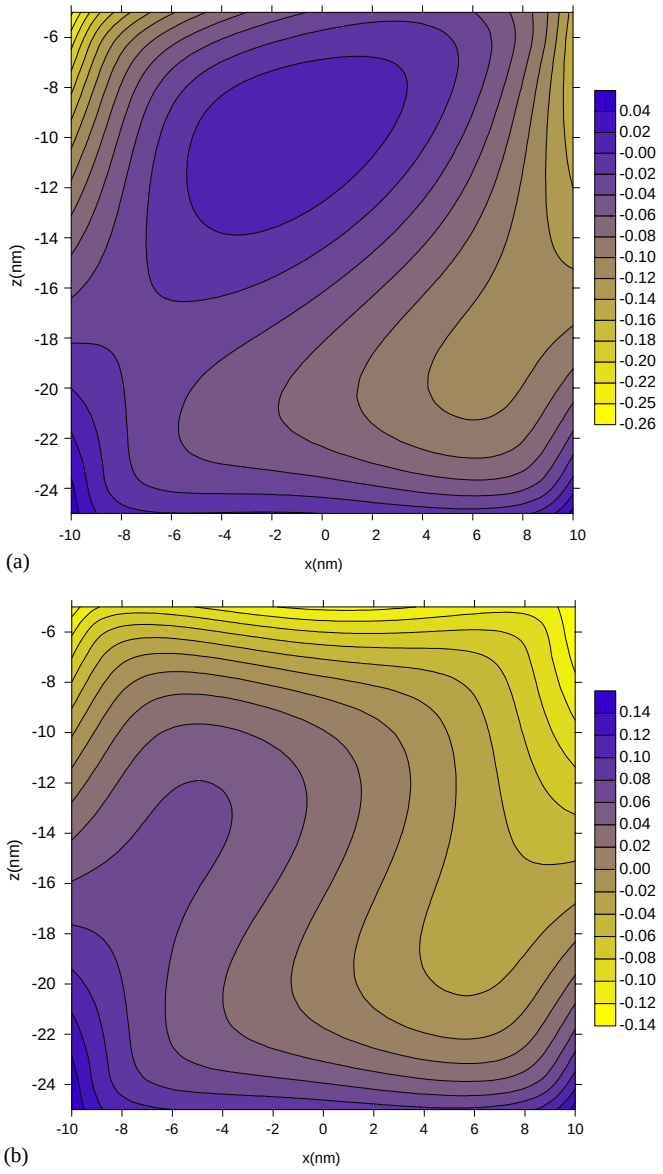

Fig. 8. Contours of piezoelectric potential ϕ (in V) for boundary condition Case I (a) and Case II (b) in a square QWR of 20 nm $\times$ 20 nm within the GaAs (111) full-plane.

half-plane. As can be seen, the contours for both cases are completely different in terms of their shapes and magnitudes, with both of them being also distinct to that in the full-plane (Fig. 4). In particular, it is noted that the magnitude of the potential in Case I is roughly twice that in Case II (0.26 vs. 0.14).

7. Conclusions

In this paper, we derived an exact closed-form solution for the Eshelby problem of polygonal inclusions in anisotropic piezoelectric full- and half-planes, assuming a uniform extended eigenstrain field. Based on the equivalent body-force concept of eigenstrain, we expressed the induced elastic and piezoelectric fields in terms of a line integral on the boundary of the inclusion with the integrand being the line-source Green's function. Using the recently derived exact closed-form Green's function, the line integral is carried out analytically by assuming a piecewise straight-line boundary for the inclusion, i.e., an arbitrarily shaped polygon. The most remarkable feature is that the final result involves only very simple elementary functions. The solution is then applied to a square QWR within the GaAs full- and half-planes, with results clearly showing the importance of material orientation and piezoelectric coupling. While the numerical results can also serve as benchmarks and could be useful to the analysis of nanoscale QWR structures, the corresponding multiply inclusion problem or an array of QWRs in the piezoelectric semiconductor substrate can be performed readily using the present exact closed-form solution.

Acknowledgements

The author is grateful to Dr. Gregory Rodin at The University of Texas at Austin, Dr. Frank Glas at Laboratoire de Photonique et de nanostructures of France, and Dr. David Faux at University of Surrey of UK for kindly sharing their exact isotropic results. Communications with them have been very beneficial to this author. One of the reviewers made several valuable comments, which have been incorporated into the manuscript. Dr. Nozaki kindly provided the author with a copy of his recent paper (Nozaki et al., 2001). This project was supported partially by The University of Akron under Grant No. 2-07522.

Appendix A. Stroh Eigenvalues p_J and Eigenmatrices A and B

The eigenvalue p and eigenvector $\boldsymbol{a}$ appearing in Eq. (15) satisfy the following eigenrelation in the (x,z)-plane:

$$[\boldsymbol{Q} + p(\boldsymbol{R} + \boldsymbol{R}^{\mathrm{T}}) + p^2\boldsymbol{T}]\boldsymbol{a} = 0, \tag{A.1}$$

where the superscript T denotes matrix transpose, and

$$Q_{IK} = C_{1IK1}, \quad R_{IK} = C_{1IK3}, \quad T_{IK} = C_{3IK3} \tag{A.2}$$

with

$$\boldsymbol{b} = (\boldsymbol{R}^{\mathrm{T}} + p\boldsymbol{T})\boldsymbol{a} = -\frac{1}{p}(\boldsymbol{Q} + p\boldsymbol{R})\boldsymbol{a}. \tag{A.3}$$

Denoting by p_m, $\boldsymbol{a}_m$, and $\boldsymbol{b}_m$ $(m = 1,2,\ldots,8)$ the eigenvalues and the associated eigenvectors of Eq. (A.1), we can order them in a way so that

$$\text{Im } p_J > 0,\ p_{J+4} = \bar{p}_J, \quad \boldsymbol{a}_{J+4} = \bar{\boldsymbol{a}}_J, \quad \boldsymbol{b}_{J+4} = \bar{\boldsymbol{b}}_J \quad (J = 1,2,3,4),$$

$$\boldsymbol{A} = [\boldsymbol{a}_1, \boldsymbol{a}_2, \boldsymbol{a}_3, \boldsymbol{a}_4], \quad \boldsymbol{B} = [\boldsymbol{b}_1, \boldsymbol{b}_2, \boldsymbol{b}_3, \boldsymbol{b}_4], \tag{A.4}$$

where Im stands for the imaginary part of a complex variable and an over-bar for the complex conjugate. We assume that the eigenvalues p_J are distinct and the eigenvectors $\boldsymbol{a}_J$, and $\boldsymbol{b}_J$ satisfy the normalization relation (Barnett and Lothe, 1975; Ting, 1996)

$$\boldsymbol{b}_I^{\mathrm{T}}\boldsymbol{a}_J + \boldsymbol{a}_I^{\mathrm{T}}\boldsymbol{b}_J = \delta_{IJ} \tag{A.5}$$

with δ_{IJ} being the 4×4 Kronecker delta, i.e., the 4×4 identity matrix. We also remark that repeated eigenvalues p_J can be avoided by using slightly perturbed material coefficients with negligible errors (Pan, 1997). In doing so, the simple structure of the solution presented in the text can always be utilized.

References

Andreev, A.D., Downes, J.R., Faux, D.A., O'Reilly, E.P., 1999. Strain distribution in quantum dots of arbitrary shape. J. Appl. Phys. 86, 297–305.

Bacon, D.J., Barnett, D.M., Scattergood, R.O., 1978. The anisotropic continuum theory of lattice defects. Prog. Mater. Sci. 23, 51–262.

Barnett, D.M., Lothe, J., 1975. Dislocations and line charges in anisotropic piezoelectric insulators. Phys. Stat. Sol. (b) 67, 105–111.

Buryachenko, V.A., 2001. Multiparticle effective field and related methods in micromechanics of composite materials. Appl. Mech. Rev. 54, 1–47.

Chung, M.Y., Ting, T.C.T., 1996. Piezoelectric solid with an elliptic inclusion or hole. Int. J. Solids Struct. 33, 3343–3361.

Davies, J.H., 1998. Elastic and piezoelectric fields around a buried quantum dot: a simple picture. J. Appl. Phys. 84, 1358–1365.

Davies, J.H., Larkin, I.A., 1994. Theory of potential modulation in lateral surface superlattices. Phys. Rev. B 49, 4800–4809.

Dong, C.Y., Lo, S.H., Cheung, Y.K., 2003. Stress analysis of inclusion problems of various shapes in an infinite anisotropic elastic medium. Comput. Meth. Appl. Mech. Eng. 192, 683–696.

Downes, J.R., Faux, D.A., O'Reilly, E.P., 1995. Influence of strain relaxation on the electronic properties of buried quantum wells and wires. Mater. Sci. Eng. B35, 357–363.

Dunn, M.L., Taya, M., 1993. An analysis of piezoelectric composite materials containing ellipsoidal inhomogeneities. Proc. R. Soc. Lond. A443, 265–287.

Dunn, M.L., Wienecke, H.A., 1997. Inclusions and inhomogeneities in transversely isotropic piezoelectric solids. Int. J. Solids Struct. 34, 3571–3582.

Eshelby, J.D., 1957. The determination of the elastic field of an ellipsoidal inclusion, and related problems. Proc. R. Soc. Lond. A241, 376–396.

Eshelby, J.D., 1961. Elastic inclusions and inhomogeneities. In: Sneddon, I.N., Hill, R. (Eds.), Vol. 2, Progress in Solid Mechanics North-Holland, Amsterdam, pp. 89–140.

Faux, D.A., Pearson, G.S., 2000. Green's tensors for anisotropic elasticity: application to quantum dots. Phys. Rev. B 62, R4798–R4801.

Faux, D.A., Downes, J.R., O'Reilly, E.P., 1996. A simple method for calculating strain distribution in quantum-wire structures. J. Appl. Phys. 80, 2515–2517.

Faux, D.A., Downes, J.R., O'Reilly, E.P., 1997. Analytic solutions for strain distribution in quantum-wire structures. J. Appl. Phys. 82, 3754–3762.

Freund, L.B., 2000. The mechanics of electronic materials. Int. J. Solids Struct. 37, 183–196.
Freund, L.B., Gosling, T.J., 1995. Critical thickness for growth of strained quantum wires in substrate V-grooves. Appl. Phys. Lett. 66, 2822–2824.
Glas, F., 2001. Elastic relaxation of truncated pyramidal quantum dots and quantum wires in a half-space: an analytical calculation. J. Appl. Phys. 90, 3232–3241.
Glas, F., 2002a. Analytical calculation of the strain field of single and periodic misfitting polygonal wires in a half-space. Philos. Mag. A82, 2591–2608.
Glas, F., 2002b. Elastic relaxation of isolated and interacting truncated pyramidal quantum dots and quantum wires in a half space. Appl. Surf. Sci. 188, 9–18.
Glas, F., 2003. Elastic relaxation of a truncated circular cylinder with uniform dilatational eigenstrain in a half space. Phys. Stat. Sol. B 237, 599–610.
Gosling, T.J., Willis, J.R., 1995. Mechanical stability and electronic properties of buried strained quantum wire arrays. J. Appl. Phys. 77, 5601–5610.
Ju, J.W., Sun, L.Z., 2001. Effective elastoplastic behavior of metal matrix composites containing randomly located aligned spheroidal inhomogeneities. Part I: micromechanics-based formulation. Int. J. Solids Struct. 38, 183–201.
Kawashita, M., Nozaki, H., 2001. Eshelby tensor of a polygonal inclusion and its special properties. J. Elasticity 64, 71–84.
Kogan, L., Hui, C.Y., Molkov, V., 1996. Stress and induction field of a spheroidal inclusion or a penny-shaped crack in a transversely isotropic piezoelectric material. Int. J. Solids Struct. 33, 2719–2737.
Kouris, D.A., Mura, T., 1989. The elastic field of a hemispherical inhomogeneity at the free surface of an elastic half space. J. Mech. Phys. Solids 37, 365–379.
Larkin, I.A., Davies, J.H., Long, A.R., Cusco, R., 1997. Theory of potential modulation in lateral surface superlattices. II. Piezoelectric effect. Phys. Rev. B 56, 15242–15251.
Lu, P., Williams, F.W., 1998. Green's functions of piezoelectric material with an elliptic hole or inclusion. Int. J. Solids Struct. 35, 651–664.
Markenscoff, X., 1993. On the Dundurs correspondence between cavities and rigid inclusions. J. Appl. Mech. 60, 260–264.
Markenscoff, X., 1998a. Inclusions of uniform eigenstrains and constant or other stress dependence. J. Appl. Mech. 65, 863–866.
Markenscoff, X., 1998b. Inclusions with constant eigenstress. J. Mech. Phys. Solids 46, 2297–2301.
Michelitsch, T.M., Gao, H., Levin, V.M., 2003. Dynamic Eshelby tensor and potentials for ellipsoidal inclusions. Proc. R. Soc. Lond. A459, 863–890.
Mura, T., 1987. Micromechanics of Defects in Solids, 2nd Revised Edition. Kluwer Academic Publishers, Dordrecht.
Nozaki, H., Taya, M., 1997. Elastic fields in a polygon-shaped inclusion with uniform eigenstrains. J. Appl. Mech. 64, 495–502.
Nozaki, H., Taya, M., 2001. Elastic fields in a polyhedral inclusion with uniform eigenstrains and related problems. J. Appl. Mech. 68, 441–452.
Nozaki, H., Horibe, T., Taya, M., 2001. Stress field caused by polygon inclusion. JSME Int. J. Series A 44, 472–482.
Pan, E., 1997. A general boundary element analysis of 2-D linear elastic fracture mechanics. Int. J. Fract. 88, 41–59.
Pan, E., 1999. A BEM analysis of fracture mechanics in 2D anisotropic piezoelectric solids. Eng. Anal. Bound. Elements 23, 67–76.
Pan, E., 2002a. Elastic and piezoelectric fields around a quantum dot: fully coupled or semi-coupled model? J. Appl. Phys. 91, 3785–3796.
Pan, E., 2002b. Elastic and piezoelectric fields in substrates GaAs (001) and GaAs (111) due to a buried quantum dot. J. Appl. Phys. 91, 6379–6387.
Pan, E., 2002c. Mindlin's problem for an anisotropic piezoelectric half space with general boundary conditions. Proc. R. Soc. Lond. A 458, 181–208.
Park, S., Chuang, S., 1998. Piezoelectric effects on electrical and optical properties of wurtzite GaN/AlGaN quantum well lasers. Appl. Phys. Lett. 72, 3103–3105.

Pearson, G.S., Faux, D.A., 2000. Analytical solutions for strain in pyramidal quantum dots. J. Appl. Phys. 88, 730–736.

Rahman, M., 1999a. Some problems of a rigid elliptical disk-inclusion bonded inside a transversely isotropic space: part I. J. Appl. Mech. 66, 612–620.

Rahman, M., 1999b. Some problems of a rigid elliptical disk-inclusion bonded inside a transversely isotropic space (Part II): solution of the integral equations. J. Appl. Mech. 66, 621–630.

Rahman, M., 2001. On the Newtonian potentials of heterogeneous ellipsoids and elliptical discs. Proc. R. Soc. Lond. A 457, 2227–2250.

Rahman, M., 2002. The isotropic ellipsoidal inclusion with a polynomial distribution of eigenstrain. J. Appl. Mech. 69, 593–601.

Rodin, G.J., 1996. Eshelby's inclusion problem for polygons and polyhedra. J. Mech. Phys. Solids 44, 1977–1995.

Ru, C.Q., 1999. Analytical solution for Eshelby's problem of an inclusion of arbitrary shape in a plane or half-plane. J. Appl. Mech. 66, 315–322.

Ru, C.Q., 2000. Eshelby's problem for two-dimensional piezoelectric inclusions of arbitrary shape. Proc. R. Soc. Lond. A 456, 1051–1068.

Sharma, P., Sharma, R., 2003. On the Eshelby's inclusion problem for ellipsoids with nonuniform dilatational Gaussian and exponential eigenstrains. J. Appl. Mech. 70, 418–425.

Smith, D.L., 1986. Strain-generated electric fields in [111] growth axis strained-layer superlattices. Solid State Commun. 57, 919–921.

Suo, Z., Kuo, C.M., Barnett, D.M., Willis, J.R., 1992. Fracture mechanics for piezoelectric ceramics. J. Mech. Phys. Solids 40, 739–765.

Tiersten, H.F., 1969. Linear Piezoelectric Plate Vibrations. Plenum, New York.

Ting, T.C.T., 1996. Anisotropic Elasticity. Oxford University Press, Oxford.

Walpole, L.J., 1991. A translated rigid ellipsoidal inclusion in an elastic medium. Proc. R. Soc. Lond. A 434, 571–585.

Wang, B., 1992. Three-dimensional analysis of an ellipsoidal inclusion in a piezoelectric material. Int. J. Solids Struct. 29, 293–308.

Wang, X., Shen, Y.P., 2003. Inclusions of arbitrary shape in magnetoelectroelastic composite materials. Int. J. Eng. Sci. 41, 85–102.

Willis, J.R., 1981. Variational and related methods for the overall properties of composites. Advances Appl. Mech. 21, 1–78.

Withers, P.J., 1989. The determination of the elastic field of an ellipsoidal inclusion in a transversely isotropic medium, and its relevance to composite materials. Philos. Mag. A 59, 759–781.

Yu, H.Y., Sanday, S.C., 1991. Elastic field in joined semi-infinite solids with an inclusion. Proc. R. Soc. Lond. A 434, 521–530.

Yu, H.Y., Sanday, S.C., Chang, C.I., 1994. Elastic inclusion and inhomogeneities in transversely isotropic solids. Proc. R. Soc. Lond. A 444, 239–252.